

Journal of Biomedical Optics

SPIEDigitalLibrary.org/jbo

Detection of intestinal dysplasia using angle-resolved low coherence interferometry

Neil Terry
Yizheng Zhu
Julie K. M. Thacker
John Migaly
Cynthia Guy
Christopher R. Mantyh
Adam Wax

Detection of intestinal dysplasia using angle-resolved low coherence interferometry

Neil Terry,^a Yizheng Zhu,^a Julie K. M. Thacker,^b John Migaly,^c Cynthia Guy,^d Christopher R. Mantyh,^e and Adam Wax^a

^aDuke University, Department of Biomedical Engineering, 136 Hudson Hall, Durham, North Carolina 27708

^bDuke University, Department of Surgery, DUMC 2829, Durham, North Carolina 27710

^cDuke University, Department of Surgery, DUMC 2817, Durham, North Carolina 27710

^dDuke University, Department of Pathology, DUMC 3712, Durham, North Carolina 27710

^eDuke University, Department of Surgery, DUMC 3117, Durham, North Carolina 27710

Abstract. Angle-resolved low coherence interferometry (a/LCI) is an optical biopsy technique that allows for depth-resolved, label-free measurement of the average size and optical density of cell nuclei in epithelial tissue to assess the tissue health. a/LCI has previously been used clinically to identify the presence of dysplasia in Barrett's Esophagus patients undergoing routine surveillance. We present the results of a pilot, *ex vivo* study of tissues from 27 patients undergoing partial colonic resection surgery, conducted to evaluate the ability of a/LCI to identify dysplasia. Performance was determined by comparing the nuclear morphology measurements with pathological assessment of co-located physical biopsies. A statistically significant correlation between increased average nuclear size, reduced nuclear density, and the presence of dysplasia was noted at the basal layer of the epithelium, at a depth of 200 to 300 μm beneath the tissue surface. Using a decision line determined from a receiver operating characteristic, a/LCI was able to separate dysplastic from healthy tissues with a sensitivity of 92.9% (13/14), a specificity of 83.6% (56/67), and an overall accuracy of 85.2% (69/81). The study illustrates the extension of the a/LCI technique to the detection of intestinal dysplasia, and demonstrates the need for future *in vivo* studies. © 2011 Society of Photo-Optical Instrumentation Engineers (SPIE). [DOI: 10.1117/1.3631799]

Keywords: a/LCI; light scattering; intestinal dysplasia; early cancer detection; optical biopsy.

Paper 11202R received Apr. 21, 2011; revised manuscript received Jun. 29, 2011; accepted for publication Aug. 9, 2011; published online Oct. 3, 2011.

1 Introduction

Colorectal cancer (CRC) is one of the leading causes of death in the United States today. While incidence and mortality rates associated with this disease have decreased over time, it continues to affect over 154,000 individuals annually.¹ It is well-established that early detection of adenomatous tissue reduces the mortality and morbidity of colorectal adenocarcinomas. The acceptance of universal screening for adenomas and dysplastic tissue via colonoscopy has indeed led to a significant reduction in colorectal cancer mortality in the last 10 years.² However, despite recent advances in colonoscopy techniques, adenoma miss rates of up to 30% have been reported in routine colonoscopies.³ The small size and low profile of early dysplasias are largely responsible for this miss rate, as these lesions are difficult to identify with white light endoscopic tools. Because of the benefit of finding these small, early-stage dysplasias, improved surveillance methods are needed.

Several difficulties arise from the reliance on a physical biopsy for identification and pathological evaluation of potential dysplasias during colonoscopies. First, the need for subsequent processing and evaluation of physical biopsies introduces a time delay to diagnosis, as the sample must be fixed and stained before it can be independently evaluated by a pathologist. This time delay necessitates an additional procedure to take therapeutic action in the case of an incipient cancer. While system-

atic physical biopsies are typically used for monitoring patients with an increased risk for developing CRC, the detection of flat dysplasias is particularly difficult using this approach because of their low visibility and the need to cover large tissue areas.⁴ Another concern with relying on evaluation of biopsies is the subjective nature of histopathology, which can also lead to classification error. For example, sampling errors during endoscopic biopsies of large adenomas may miss invasive cancers. It has been shown that interobserver agreement when evaluating colorectal tissue for signs of dysplasia is moderate.⁵ There is a clear need for surveillance tools that can provide real-time, objective assessments of colorectal tissue health.

Optical techniques that analyze the light scattering signature of the intestinal epithelium have been introduced as potential guides to a biopsy.⁶⁻¹⁰ These techniques are able to provide information regarding the tissue substructure, which can serve as biomarkers for the presence of intraepithelial neoplasia. Recently, Backman and Roy have proposed measurement of the field effect of colon carcinogenesis using light scattering techniques as a means of risk stratification and prescreening for CRC.¹¹ Additionally, optical coherence tomography (OCT), a depth-resolved optical imaging technique, has been used to image the microstructure of intestinal epithelium during endoscopy to evaluate tissue health.¹²⁻¹⁴

Angle-resolved low coherence interferometry (a/LCI) is a light scattering technique that combines the abilities of light scattering spectroscopy to detect morphological changes in cell nuclei with the depth-resolving power of OCT. The technique

Address all correspondence to: Neil Terry, Duke University, Department of Biomedical Engineering, 136 Hudson Hall, Box 90281, Durham, NC 27708; Tel: 919-613-9144; Fax: 919-613-1944; E-mail: neil.terry@duke.edu.

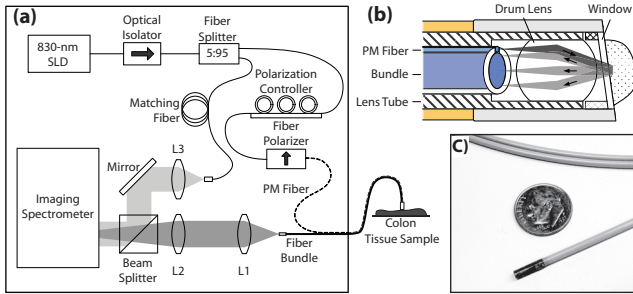


Fig. 1 a/LCI system diagram. (a) System illustration, (b) probe tip assembly illustration showing delivered (dark gray) and scattered (light gray) light, and (c) photograph of the endoscopic probe pictured next to a U.S. dime for scale. Illustration adapted from Zhu et al. (Ref. 22).

has been used to identify intraepithelial neoplasia in multiple models.^{15–18} Recently, a/LCI has shown the ability to detect dysplasia in the epithelium of human esophagus.^{19–21} This study evaluates the ability of a/LCI to detect dysplasia *in situ* in epithelial tissue samples from a human colon following surgical resection.

2 Patients and Methods

2.1 Instrumentation

The experiments were conducted with a clinically compatible endoscopic a/LCI system (Fig. 1) that has been previously introduced.²² Fiber-optic coupled light generated by an 830-nm superluminescent diode (Superlum Diodes, Moscow, Russia, $\Delta\lambda_{\text{FWHM}} = 19$ nm) passes through an optical isolator (AC Photonics, California) and is split into reference and sample arms at a 5:95 ratio by a fiber splitter (AC Photonics, California). A polarization controller (Thorlabs, New Jersey) is used in the sample arm in order to maximize the power coupled by a fiber polarizer (Chiral Photonics, Inc., New Jersey) into a polarization-maintaining delivery fiber (Corning, Inc., New York); the use of polarized light in the sample arm of a/LCI systems has been previously shown to improve their ability to size particles accurately.²³ The polarized light is transmitted through the fiber probe assembly to the probe tip [Fig. 1(b)], where it is delivered to the sample as a collimated light beam (0.5-mm diameter) at an oblique angle by a drum lens (diameter: 1.5 mm, length: 2.5 mm; Edmund Optics, New Jersey). The delivered light passes through a protective window that is angled 8 deg out-of-plane in order to prevent reflected light from being collected. The angular distribution of the scattered light is imaged across the face of a coherent imaging fiber bundle (Schott NA, New York) placed in the Fourier plane at the back focal plane of the drum lens. By using a 4f system comprised of lenses L1 and L2 to image the proximal face of the fiber bundle onto the input slit of an imaging spectrometer (Spectrapro 2150i; Acton Research Corporation, Massachusetts), the spectral profile of the angular distribution of scattered light collected across a strip through the center of the fiber bundle is collected by a CCD (Pixis:100; Princeton Instruments, New Jersey). Reference light that has passed through a pathlength-matched single-mode optical fiber and been collimated by L3 is mixed with the sample beam at a beam splitter in order to produce spectral interference fringes whose frequency is a function of pathlength mismatch

between the two arms. These interference fringes are processed in a manner similar to Fourier-domain OCT to produce individual depth scans for each scattered angle in a procedure previously described by Brown et al.²¹

2.2 Study Design

Twenty-seven subjects undergoing partial colonic resection surgery at Duke University Medical Center were enrolled in this study. For each subject, the tissue sample was opened longitudinally and multiple (typically 5 to 6) epithelial locations were evaluated using the a/LCI probe within 2 h of resection for a total of 138 paired biopsy locations. Scan locations were selected on the margins of the gross lesions in an effort to find dysplastic tissue sites. An additional single scan was taken from each tissue sample at a remote location, believed to contain healthy tissue upon gross examination. At each measurement point, the probe was brought into contact with the tissue and 15 to 25 acquisitions of 25 ms each were taken. All scans for each single optical biopsy were collected in under 30 s. Across all patients, a total of 2734 individual scattering spectra were acquired. Following imaging using the a/LCI system, India ink was used to mark the sampled points and physical biopsies were collected for histopathological analysis. The samples were analyzed to determine the disease state by a trained pathologist. This study was conducted with the oversight of the Institutional Review Board at the Duke University Medical Center in Durham, North Carolina.

2.3 Data Processing

The a/LCI data were processed in a manner described previously in order to determine depth-resolved nuclear morphology characteristics of the epithelial tissue.^{19,21,22} Briefly, the data were processed to isolate the scattering components from cell nuclei in three depth segments of the tissue: the segment from the tissue surface to 100 μm in depth, the segment between 100 and 200 μm in depth, and the segment from 200 to 300 μm in depth, identified as the basal layer of the epithelium. Periodic oscillations in the angular spectra, which are characteristic of the underlying nuclear morphology, were compared to theoretical predictions to determine the average nuclear diameter and nuclear density of the tissue in question. In this analysis, nuclear density is measured as the relative ratio of the average refractive index of the cell nuclei and the surrounding cytoplasm. Each scan was examined to ensure a scattering signature of sufficient strength, and those that did not fulfill this requirement were rejected. Morphological characteristics, as measured using a/LCI, were compared to pathologic classification of co-registered tissue samples as determined by a trained pathologist.

Statistical analyses were used to assess the association of dysplasia with the a/LCI measurements of nuclear morphology. For each model, the pathologic diagnosis was dichotomized as dysplasia versus no dysplasia. Statistical significance was determined between average nuclear morphological characteristics as measured by a/LCI for dysplastic and nondysplastic biopsies, which are given below as the mean value with the standard deviation noted in parentheses (SD). Normality of these data was verified using the Shapiro–Wilk W-test. For normally-distributed data, the Student’s t-test was used to

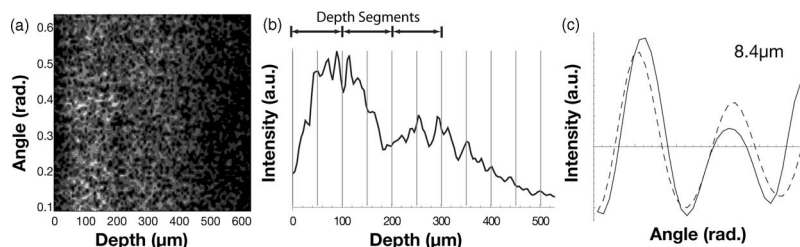


Fig. 2 Typical a/LCI data. (a) Angle-resolved depth scan of light scattered from tissue. Lighter shades of gray indicate an increased amount of scattered light. (b) A-scan indicating depth increments used for processing. Fifty micrometer segments of the tissue used for processing are indicated. (c) Example angular scan pictured (solid line) with best-fit Mie theory solution (dashed line) and size indicated.

assess statistical significance. For data that were not normally distributed, the Wilcoxon Rank Sum test was used. *P* values associated with type I error rates of less than 0.05 were considered significant in this study. All analyses were performed using JMP version 9.0 (SAS Institute, Inc., Cary, North Carolina).

The relationship between sensitivity and specificity was determined through the development of a receiver operating characteristic (ROC) for each of the three epithelial depth layers. For these analyses, the presence of dysplasia was considered a binary classifier and nuclear diameter and density were used as discriminants. To evaluate the predictive ability of these measures, an area under the ROC curve (AUC) was calculated as a fraction of the maximum possible AUC.

3 Results

3.1 Sample Data

Typical a/LCI data are shown in Fig. 2. Figure 2(a) shows an angle- and depth-resolved scattering map, which contains the angular distribution of light scattered by the sample as resolved by depth. Light shades of gray indicate higher intensities, which correspond to increased amounts of scattered light. The horizontal axis indicates depth in the sample, with 0 μm corresponding to the interface between the probe and the tissue. A depth-resolved reflection profile is created by summing across the angular range of the scattering map [Fig. 2(b)]. During signal processing, the angular scattering pattern is analyzed in 50- μm segments, indicated by gray lines. Fig. 2(c) shows an example

angular profile recovered from a single 50- μm depth segment between 200 and 250 μm beneath the epithelial surface of healthy tissue. This angular profile (solid line) is overlaid with the best theoretical fit (dashed line). The corresponding average nuclear size for this depth segment of tissue is indicated.

3.2 Biopsy Results

Of the 27 tissue samples examined with the a/LCI system, histological evaluation showed that 8 were pathologically normal, 7 presented for low- and high-grade dysplasia, 2 showed both dysplasia and adenocarcinoma, 5 displayed only invasive adenocarcinoma, and 5 were characterized as ulcerative diseases. In the presented analysis, only biopsies that were pathologically normal or that had a diagnosis of low- (LGD) or high-grade (HGD) dysplasia were considered. This restriction resulted in a data set that consisted of 14 dysplastic biopsies from adenomatous polyps (both LGD and HGD) and 67 biopsies from healthy tissue sites, with 26.4% of acquired scans omitted due to low signal strength.

3.3 Statistical Analyses

Nuclear diameter and density were measured at each of three epithelial depth segments. These results are given in Table 1. All data were normally-distributed, with the exception of the nuclear density of pathologically-normal biopsies from 0 to 100 μm in depth and the nuclear diameter of dysplastic biopsies

Table 1 Average nuclear morphology measurements at each of the 100- μm epithelial depth segments for nondysplastic and dysplastic biopsies as measured by a/LCI. Data are given as mean (SD) and statistical significance as indicated with associated *p*-value. NS indicates that the specified characteristic was unable to differentiate dysplasia at a statistically-significant level ($P < 0.05$). Single and triple asterisks indicate statistical significance at the $P < 0.05$ and $P < 0.001$ level, respectively.

	Nondysplastic ($n = 67$)	Dysplastic ($n = 14$)	Statistical significance
Nuclear diameter (0 to 100 μm)	9.73 μm (1.43 μm)	9.52 μm (1.23 μm)	NS ($p = 0.29$)
Nuclear density (0 to 100 μm)	1.042 (0.0036)	1.044 (0.0058)	NS ($p = 0.64$)
Nuclear diameter (100 to 200 μm)	10.52 μm (1.36 μm)	9.64 μm (1.61 μm)	* ($p = 0.036$)
Nuclear density (100 to 200 μm)	1.043 (0.0036)	1.044 (0.0045)	NS ($p = 0.36$)
Nuclear diameter (200 to 300 μm)	9.29 μm (1.28 μm)	11.58 (1.36 μm)	*** $p < 0.0001$
Nuclear density (200 to 300 μm)	1.045 (0.0040)	1.041 (0.0028)	*** $p < 0.0001$

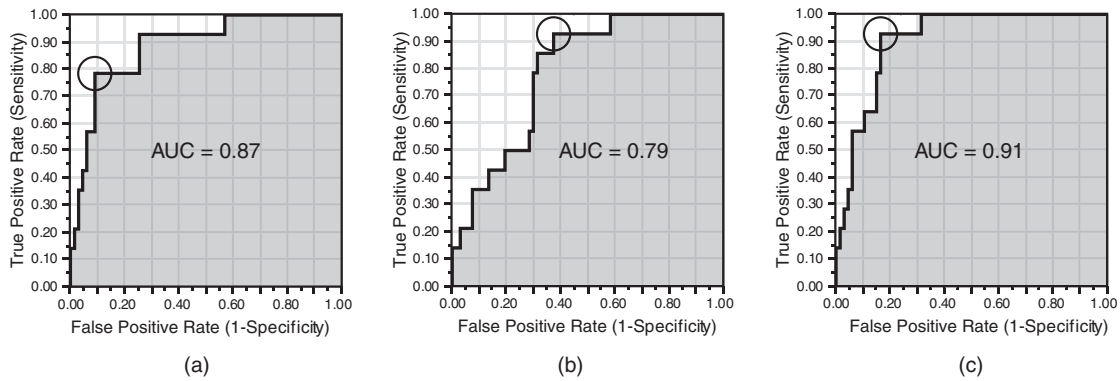


Fig. 3 ROC curves corresponding to various discriminators for the third 100- μm segment of the epithelium. AUC (gray area) ratios are indicated. Circles indicate optimal value for each discriminator. (a) Nuclear diameter, AUC = 0.87; (b) nuclear density, AUC = 0.79; (c) nuclear diameter and nuclear density, AUC = 0.91.

from 100 to 200 μm in depth. Measurements of nuclear diameter and density between the epithelial surface and a depth of 100 μm did not differ in a statistically-significant manner, nor did nuclear density between 100 and 200 μm . A decrease in nuclear diameter between 100 and 200 μm was statistically associated with the presence of dysplasia at the $p < 0.05$ level. For the depth layer between 200 and 300 μm , both a reduced nuclear density and an increased nuclear diameter were statistically associated with the presence of dysplasia at the $p < 0.0001$ level.

To determine the relationship between sensitivity and specificity, ROC curves were created using each of the six nuclear morphological measurements as discriminants. For these analyses, the presence of dysplasia was considered as a binary classifier. Nuclear diameter and density of tissue from the epithelial depth of 200 to 300 μm demonstrated a good ability to predict

the presence of dysplasia, and were individually associated with AUC values of 0.87 and 0.79, respectively. When these measures were linearly combined to form a single discriminator, a ROC with an AUC of 0.91 was obtained. The three aforementioned ROC curves for the 200 to 300 μm depth segment appear in Fig. 3. To a lesser extent, average nuclear diameter of tissue located 100 to 200 μm beneath the mucosal surface was effective at discriminating between dysplastic and nondysplastic populations, with an AUC value of 0.68. Neither the average nuclear diameter of tissue between 0 and 100 μm in depth (AUC = 0.54), the average nuclear density of tissue between 0 and 100 μm (AUC = 0.53), nor the average nuclear density of tissue between 100 and 200 μm (AUC = 0.56) were able to effectively detect dysplasia.

A scatter plot of average nuclear diameter and nuclear density for the epithelium from 200 to 300 μm in depth is shown in Fig. 4. Because both nuclear diameter and nuclear density are statistically-significant predictors of the presence of dysplasia, it is possible to draw an optimal decision line (dashed line in Fig. 4) as determined by ROC analysis that efficiently and accurately distinguishes the dysplastic biopsies, which have increased nuclear diameter and decreased nuclear density, from those that are pathologically normal. This optimal discriminator corresponds to the point on the ROC curve that is geometrically closest to the upper left, which represents perfect sensitivity and specificity. By using this decision line, which is nearly identical to that previously determined by Pytila et al.,²⁰ the biopsies can be classified with a sensitivity of 92.9% (13/14), a specificity of 83.6% (56/67), and an overall accuracy of 85.2% (69/81). Furthermore, this decision line yields a positive-predictive value of 54.2% (13/24) and a negative-predictive value of 98.2% (56/57).

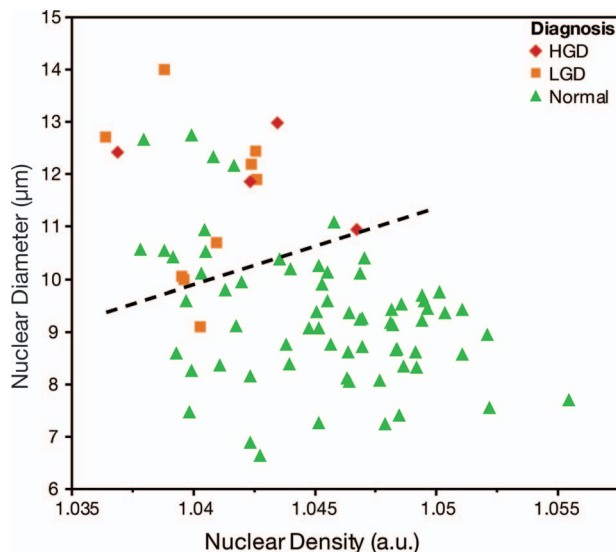


Fig. 4 Scatter plot showing nuclear size (micrometer) versus nuclear density for the epithelial depth segment 200 to 300 μm beneath the mucosal surface. Each point represents a single optical biopsy, and points are color-coded with respect to their pathological assessment. The dashed black line indicates the ideal decision line for these data for the prediction of dysplasia.

4 Discussion

In this study, the depth segment of epithelial tissue located between 200 and 300 μm beneath the mucosal surface proved to be of greatest diagnostic value among the three depth segments analyzed using the a/LCI technique. While nuclear diameter and density in this layer were both statistically-significant indicators of dysplasia, a combination of these measurements provided

optimal discrimination. This result is consistent with a/LCI results from previous clinical studies. In studies evaluating the ability of a/LCI to predict the presence of dysplasia in Barrett's esophagus patients, the deep tissue layer corresponding to the basal layer of the epithelium has been proven to contain the largest amount of diagnostically relevant information.^{19,21} This is likely due to a reduced influence of confounding factors at this depth layer, such as inflammation. Furthermore, previous a/LCI studies have also identified a sloped decision line, as found here, that combines nuclear diameter and density as an optimal discriminator between dysplastic and nondysplastic optical biopsies.^{20,21}

The average nuclear diameter in the shallower segment of tissue, 100 to 200 μm in depth, also showed the ability to differentiate between dysplastic and nondysplastic tissues, albeit at a lower level of statistical significance than the measurements from the deeper layer of tissue. Notably, for this layer a decrease in nuclear size was correlated with dysplasia, rather than the increase in nuclear size that was seen for diseased tissue in the deeper tissue layer. This can be explained by considering the geometry of the delivery and collection of light by the a/LCI probe, which measures only the diameter of nuclei that appears in profile with respect to the instrument.²⁴ As the columnar tissue becomes dysplastic, cellular nuclei typically elongate and depolarize as they increase in size. While previous studies have shown that a/LCI is able to accurately size elongated nuclei, the structure of dysplastic intestinal crypts is likely to result in a measurement of the minor axis of nuclei in this layer by the a/LCI probe;^{17,25,26} this phenomenon could explain the reduced nuclear diameter measured by a/LCI in dysplastic tissue at intermediate tissue depths. Advanced a/LCI systems, with the ability to probe multiple dimensions of cell nuclei,^{27,28} are needed to further assess the complex tissue architecture found in intestinal epithelium, and may provide improved accuracy in the prediction of dysplasia. Furthermore, future studies may find that examination of additional epithelial depths may provide complementary information that allows more accurate classification of the disease state.

The a/LCI technique utilizes a probe geometry that requires tissue contact in order to ensure a consistent geometrical interface with the tissue surface. Because of this, tissue that is soft and offers little resistance to pressure, such as that associated with advanced lesions with no muscular substructure, was seen to yield poor a/LCI measurements here. While the scan rejection rate from this study is lower than that from a prior a/LCI study,¹⁹ the limited ability to acquire data from these soft masses presents a challenge in further development of the approach for this application. However, because the tissues in this study were resected due to a highly advanced disease state, these types of invasive adenocarcinomas are unlikely to be the subject of additional biopsy techniques, as they are so advanced that they would be expected to be surgically removed. Under guidance from a pathologist, efforts were made to focus the biopsies in this study on the margins of these masses, in the regions that would be expected to exhibit dysplasia rather than invasive adenocarcinoma. Instead, a/LCI could be more useful in detecting instances of flat dysplasias, such as in the case of inflammatory bowel disease, which can be difficult to identify with endoscopic imaging. Unfortunately, no cases of dysplastic inflammatory bowel disease were sampled in this study, so further study will be required

to characterize the ability of a/LCI to differentiate dysplastic lesions in these cases.

In conclusion, we have presented a preliminary study of the ability of a/LCI to detect dysplasia in *ex vivo* colon epithelial tissue in a clinical setting. Specifically, morphological characteristics of cell nuclei from the basal layer of tissue 200 to 300 μm beneath the mucosal surface were of high diagnostic value. These results indicate that a/LCI could potentially be further developed to provide a utility for assessing the health of epithelial tissue in the colon. Future studies, both of *in vivo* intestinal dysplasias and *ex vivo* flat dysplasias, would better define the clinical utility of a/LCI for assessing tissue health in the lower gastrointestinal tract.

Acknowledgments

This work was supported by the National Institutes of Health (National Cancer Institute R01-CA138594).

Adam Wax has a financial interest in Oncoscope, Inc., the company that holds proprietary rights to the technology described in this study. Neil Terry has a consulting relationship with Oncoscope, Inc.

References

1. A. Jemal, R. Siegel, J. Xu, and E. Ward, "Cancer statistics," *Ca-Cancer J. Clin.* **60**, 277–300 (2010).
2. S. J. Winawer, "The multidisciplinary management of gastrointestinal cancer. Colorectal cancer screening," *Best Pract. Res. Clin. Gastroenterol.* **21**, 1031–1048 (2007).
3. J. C. van Rijn, J. B. Reitsma, J. Stoker, P. M. Bossuyt, S. J. van Deventer, and E. Dekker, "Polyp miss rate determined by tandem colonoscopy: a systematic review," *Am. J. Gastroenterol.* **101**, 343–50 (2006).
4. T. Matsumoto, T. Kudo, Y. Jo, M. Esaki, T. Yao, and M. Iida, "Magnifying colonoscopy with narrow band imaging system for the diagnosis of dysplasia in ulcerative colitis: a pilot study," *Gastrointest. Endosc.* **66**, 957–965 (2007).
5. M. Costantini, S. Sciallero, A. Giannini, et al., "Interobserver agreement in the histologic diagnosis of colorectal polyps. the experience of the multicenter adenoma colorectal study (SMAC)." *J. Clin. Epidemiol.* **56**, 209–214 (2003).
6. H. K. Roy, Y. Liu, R. K. Wali, Y. L. Kim, A. K. Kromine, M. J. Goldberg, and V. Backman, "Four-dimensional elastic light-scattering fingerprints as preneoplastic markers in the rat model of colon carcinogenesis," *Gastroenterology* **126**, 1071–1081 (2004).
7. A. Dhar, K. S. Johnson, M. R. Novelli, S. G. Bown, I. J. Bigio, L. B. Lovat, and S. L. Bloom, "Elastic scattering spectroscopy for the diagnosis of colonic lesions: initial results of a novel optical biopsy technique," *Gastrointest. Endosc.* **63**, 257–261 (2006).
8. R. S. Gurjar, V. Backman, L. T. Perelman, I. Georgakoudi, K. Badizadegan, I. Itzkan, R. R. Dasari, and M. S. Feld, "Imaging human epithelial properties with polarized light-scattering spectroscopy," *Nat. Med.* **7**, 1245–1248 (2001).
9. H. K. Roy, A. Gomes, V. Turzhitsky, et al., "Spectroscopic microvascular blood detection from the endoscopically normal colonic mucosa: biomarker for neoplasia risk," *Gastroenterology* **135**, 1069–1078 (2008).
10. H. K. Roy, V. Turzhitsky, Y. L. Kim, et al., "Spectral slope from the endoscopically-normal mucosa predicts concurrent colonic neoplasia: a pilot ex-vivo clinical study," *Dis. Colon Rectum* **51**, 1381–1386 (2008).
11. V. Backman and H. K. Roy, "Light-scattering technologies for field carcinogenesis detection: a modality for endoscopic prescreening," *Gastroenterology* **140**, 35–41 (2011).
12. M. V. Sivak, Jr., K. Kobayashi, J. A. Izatt, A. M. Rollins, R. Ung-Runyawee, A. Chak, R. C. K. Wong, G. A. Isenberg, and J. Willis, "High-resolution endoscopic imaging of the GI tract using optical coherence tomography," *Gastrointest. Endosc.* **51**, 474–479 (2000).

13. D. C. Adler, C. Zhou, T. H. Tsai, J. Schmitt, Q. Huang, H. Mashimo, and J. G. Fujimoto, "Three-dimensional endomicroscopy of the human colon using optical coherence tomography," *Opt. Express* **17**, 784–796 (2009).
14. S. Jackle, N. Gladkova, F. Feldchtein, et al., "In vivo endoscopic optical coherence tomography of the human gastrointestinal tract—toward optical biopsy," *Endoscopy* **32**, 743–749 (2000).
15. A. Wax, J. W. Pyhtila, R. N. Graf, et al., "Prospective grading of neoplastic change in rat esophagus epithelium using angle-resolved low-coherence interferometry," *J. Biomed. Opt.* **10** (2005).
16. A. Wax, C. H. Yang, M. G. Müller, R. Nines, C. W. Boone, V. E. Steele, G. D. Stoner, R. R. Dasari, and M. S. Feld, "In situ detection of neoplastic transformation and chemopreventive effects in rat esophagus epithelium using angle-resolved low-coherence interferometry," *Cancer Res.* **63**, 3556–3559 (2003).
17. K. J. Chalut, J. H. Ostrander, M. G. Giacomelli, and A. Wax, "Light scattering measurements of subcellular structure provide noninvasive early detection of chemotherapy-induced apoptosis," *Cancer Res.* **69**, 1199–1204 (2009).
18. J. W. Pyhtila, R. N. Graf, and A. Wax, "Determining nuclear morphology using an improved angle-resolved low coherence interferometry system," *Opt. Express* **11**, 3473–3484 (2003).
19. N. G. Terry, Y. Zhu, M. T. Rinehart, et al., "Detection of dysplasia in Barrett's esophagus with in vivo depth-resolved nuclear morphology measurements," *Gastroenterology* **140**, 42–50 (2011).
20. J. W. Pyhtila, K. J. Chalut, J. D. Boyer, J. Keener, T. D'Amico, M. Gottfried, F. Gress, and A. Wax, "In situ detection of nuclear atypia in Barrett's esophagus by using angle-resolved low-coherence interferometry," *Gastrointest. Endosc.* **65**, 487–491 (2007).
21. W. J. Brown, J. W. Pyhtila, N. G. Terry, K. J. Chalut, T. A. D'Amico, T. A. Sporn, J. V. Obando, and A. Wax, "Review and recent development of angle-resolved low-coherence interferometry for detection of precancerous cells in human esophageal epithelium," *IEEE J. Sel. Top. Quantum Electron.* **14**, 88–97 (2008).
22. Y. Zhu, N. G. Terry, J. T. Woosley, N. J. Shaheen, and A. Wax, "Design and validation of an angle-resolved low-coherence interferometry fiber probe for *in vivo* clinical measurements of depth-resolved nuclear morphology," *J. Biomed. Opt.* **16**, 011003 (2011).
23. J. W. Pyhtila and A. Wax, "Polarization effects on scatterer sizing accuracy analyzed with frequency-domain angle-resolved low-coherence interferometry," *Appl. Opt.* **46**, 1735–1741 (2007).
24. A. Wax, C. H. Yang, V. Backman, K. Badizadegan, C. W. Boone, R. R. Dasari, and M. S. Feld, "Cellular organization and substructure measured using angle-resolved low-coherence interferometry," *Biophys. J.* **82**, 2256–2264 (2002).
25. M. G. Giacomelli, K. J. Chalut, J. H. Ostrander, and A. Wax, "Application of the T-matrix method to determine the structure of spheroidal cell nuclei with angle-resolved light scattering," *Opt. Lett.* **33**, 2452–2454 (2008).
26. K. J. Chalut, M. G. Giacomelli, and A. Wax, "Application of Mie theory to assess structure of spheroidal scattering in backscattering geometries," *J. Opt. Soc. Am. A* **25**, 1866–1874 (2008).
27. Y. Z. Zhu, M. G. Giacomelli, and A. Wax, "Fiber-optic interferometric two-dimensional scattering-measurement system," *Opt. Lett.* **35**, 1641–1643 (2010).
28. M. Giacomelli, Y. Z. Zhu, J. Lee, and A. Wax, "Size and shape determination of spheroidal scatterers using two-dimensional angle resolved scattering," *Opt. Express* **18**, 14616–14626 (2010).